the CEBAF FEL Group for useful discussions while generating this design. Many of the concepts employed herein originated with them. I would like to thank Christoph Leemann for several discussions over previous months, which have strongly influenced both the philosophy and execution of this design. Finally, I would like to thank Fred Dylla for his support and encouragement during this work.

References

[1] S. Benson and G. Neil, Tidewater FEL Folklore.

[2] D. Douglas, A. Hutton, Ch. Leemann and D. Neuffer, "Analytic Modeling and Lattice Scaling Relations for FEL Driver Accelerators", CEBAF-TN-95-015, 21 March 1995.

[3] *ibid.*; S. Benson and G. Neil, *op. cit.*

[4] J.J. Bisognano, C.L. Bohn, R. Li, private communications.

[5] S. Benson, private communication.

[6] H. Liu, private communication.

[7] R. Rand, Recirculating Electron Accelerators, Harwood Academic Pub., 1984.

[8] *ibid.*

[9] D. Douglas, S. Chen and J. van Zeijts, "A Lattice Design for an IR FEL Driver", CEBAF-TN-94-037, 7 July 1994.

[10] R. Rand, *op. cit.*

[11] D. Douglas, S. Chen and J. van Zeijts, *op. cit.*

[12] As noted in Note [3] of Reference [9]/[11], linac focussing during energy recovery is not exactly mirror symmetric, inasmuch as the beam energy gain is a slightly asymmetric function of phase at low energy.

[13] D. Douglas, "Preliminary Specification for IR FEL Driver Accelerator", CEBAF-TN-95-071, 8 December 1995.

[14] D. Douglas, S. Chen and J. van Zeijts, *op. cit.*

[15] D. Douglas, *op. cit.*

[16] R. Li, private communication.

The optical behavior of the return arc for different path-length and momentum compaction settings has been scanned simultaneously over ranges of ±10 cm in path length and ±0.25 m in M_{56}. At various combinations of desired path length (as set by the absolution position of the 180^o dipole in the return arc) and momentum compaction, the arc dispersion and M_{56} are set by use of trim quads; the beam is then rematched to the cryomodule using the telescope downstream of the wiggler, and the sextupole correction recomputed. Beam properties are then studied using the DIMAD tools employed above. All requirements have thereby been determined to be met over this region of parameter space.

Design Specifications

Preliminary magnetic element and diagnostic design specifications have been distributed in a companion CEBAF Technical Note, CEBAF-TN-95-071 [15]. DIMAD input and output decks defining this baseline design are available on the cebafh cluster in the following files:

~douglas/CEBAF_optics/TLFEL/irnov95/ir120695
~douglas/CEBAF_optics/TLFEL/irnov95/ir120695out

Links to on-line documentation can be found at the following World-Wide Web site.

http://www.cebaf.gov/~douglas/

Design Status

At the date of this writing, the linear and second order baseline design are complete and documented above. Higher order aberration studies of the ideal machine using TLIE are starting [16], and error sensitivity studies will commence shortly. When magnetic element, correction system, and diagnostic specifications based on above studies are completed, we will begin commissioning scenario studies. Outstanding interface issues are as follows:

- design of final bend in injection chicane
- geometry of beam trajectory in vicinity of optical cavity components
- configuration and specification of correction and diagnostic systems
- various beam dynamics issues, such as the impact of space charge, CSR, skew quad in HOM couplers, and determination of BBU thresholds
- extension of this baseline to a CSR driven option, with wiggler and matching telescopes immediately downstream of the cryomodule and a fully symmetric, large acceptance backleg transport fully recirculating the “spent” electron beam for energy recovery

Acknowledgments

I would like to thank Leigh Harwood, Andrew Hutton, Bob Legg, and all members of

Table 3: Results of particle distribution analysis for energy recovery simulation.

Initial Load

```
  PARTICLE DISTRIBUTION ANALYSIS

 3,

 AVERAGES FOR X,XP,Y,YP,L,DELTA ARE

    .20639E-05    .11948E-04   -.74474E-07    .81087E-05   -.54293E-06   -.12515E-03


 STDDEV FOR X,XP,Y,YP,L,DELTA ARE

    .22782E-03    .71997E-03    .25303E-03    .63479E-03    .59705E-03    .10169E-01



 THE FULL BEAM MATRIX IS :

    .2278E-03   .1782E-01  -.1740E-02  -.5012E-02   .1402E-01  -.2440E-02
                .7200E-03   .3019E-02  -.4483E-02  -.7269E-02  -.1312E-01
                            .2530E-03   .1122E-02   .8838E-02   .1031E-01
                                        .6348E-03   .1389E-01  -.1210E-01
                                                    .5971E-03  -.1313E-02
                                                                .1017E-01


  DETERMINANT OF FULL BEAM MATRIX * 1.0E 0 IS :
           .2555E-37
```

Final Phase Space

```
   PARTICLE DISTRIBUTION ANALYSIS

 3;

 AVERAGES FOR X,XP,Y,YP,L,DELTA ARE

    .59861E-04    .24166E-05   -.40748E-04   -.20925E-06    .10578E-04   -.48347E-03


 STDDEV FOR X,XP,Y,YP,L,DELTA ARE

    .19115E-02    .35058E-03    .21251E-02    .34838E-03    .59878E-03    .39323E-01



 THE FULL BEAM MATRIX IS :

    .1912E-02   .2712E-01  -.5201E-02   .8530E-02   .5046E-02  -.6723E-01
                .3506E-03   .1200E-01   .9704E-03  -.1114E-01   .2777E-01
                            .2125E-02  -.1506E+00  -.1629E-01   .9627E-02
                                        .3484E-03   .6262E-02   .9987E-02
                                                    .5988E-03   .8642E-01
                                                                .3932E-01
```

The energy recovery process in this system has been simulated and appears viable from the perspective of beam transport. A 6σ gaussian initial phase space load of 10000 particles was injected at the wiggler center with the nominal rms geometric emittance of 0.16 mm-mrad, an rms bunch length of 2 psec (0.6 mm) and an rms momentum spread of 1%. These rays were traced through the system with DIMAD to the end of the utility drift following the cryomodule; results at this point and at the intermediate point of maximum spot size are presented in Figure 7. RMS values for all phase space dimensions before and after the transport are given in Table 3 (which provides results from a DIMAD particle distribution analysis), and agree with the $\sigma = \sqrt{\beta\varepsilon} \sim \sqrt{5\ \text{m} \times 0.16 \times 10^{-6}\ \text{m-rad} \times (40\ \text{MeV}/10\ \text{MeV})} \sim 0.18\text{mm}$ predicted by linear transport to ~20% or better.

Figure 7: Results of raytracing simulation of energy recovery; phase spaces at peak spot size (in return arc) and at extraction point (after energy recovery)

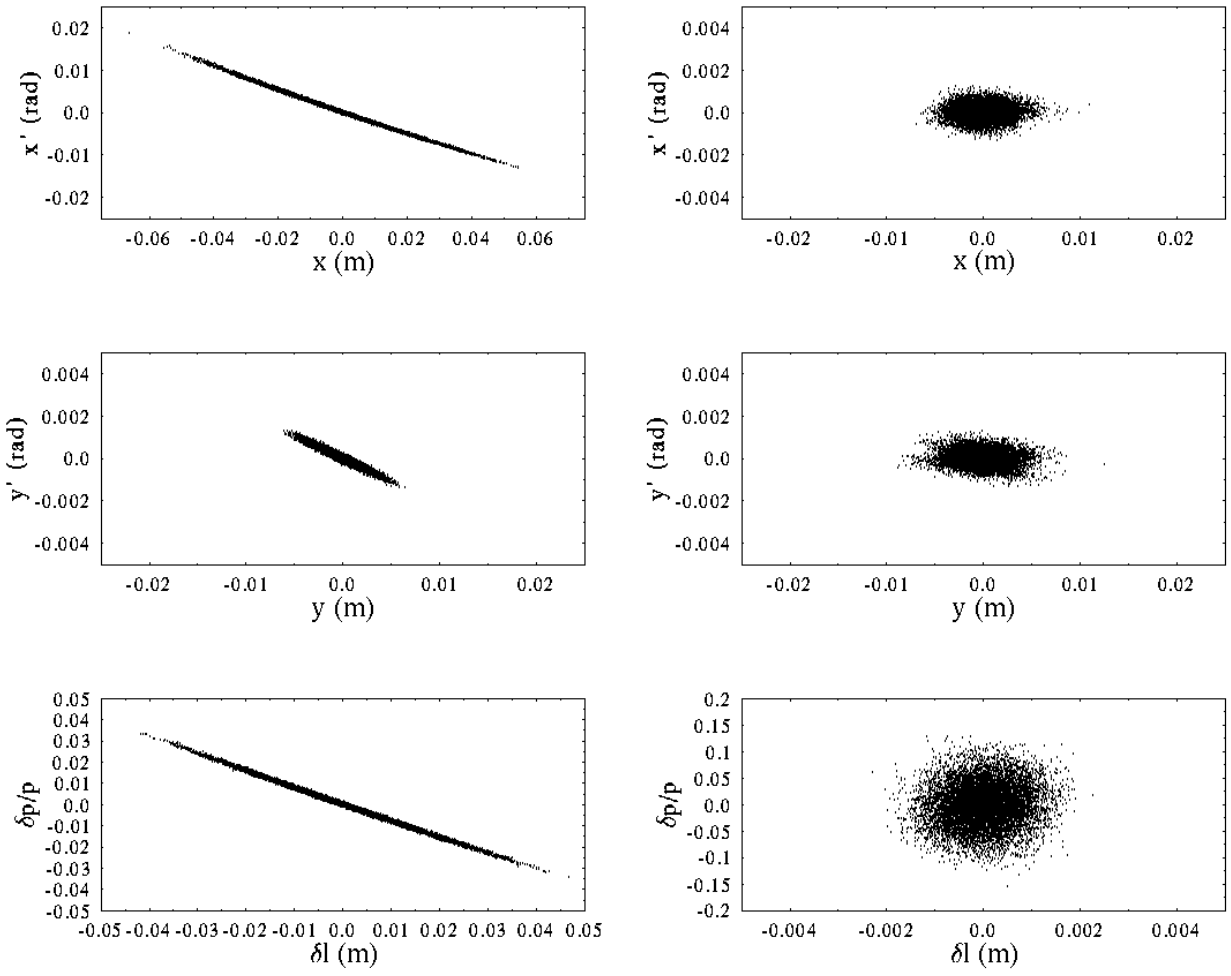

Figure 7a: At reverse bend in return arc

Figure 7b: At start of extraction chicane

Amplitude dependences of the transport have been investigated using the “line geometric aberrations” operation in DIMAD; Some results of these studies are presented in Figure 6. Figure 6a gives results of tracking from linac to wiggler several initially “matched” phase ellipses at ten times the nominal geometric emittance of 0.16 mm-mrad and momentum offsets from -3% to +3% in 1% steps; Figure 6b gives results of the equivalent simulation from wiggler to reinjection point of the linac. Both show good beam behavior over the examined region phase space, with output phase ellipses exhibiting only modest distortion. This may be quantified; the DIMAD output indicates that over the full momentum range, for ten times the nominal emittance, the relative emittance distortion $\Delta\varepsilon/\varepsilon$ in either plane is less than 0.5 in either transport.

Figure 6: Geometric aberration analysis for transport from linac to wiggler (Figure 6a) and from wiggler to linac (Figure 6b) for initially matched phase spaces at ten times the nominal geometric emittance of 0.16 mm-mrad and seven equally spaced momentum offsets on the range of ±3%.

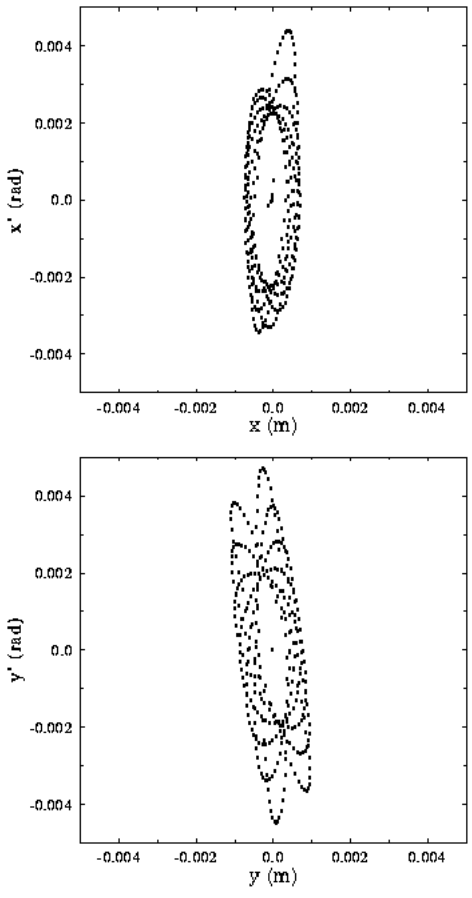

Figure 3a: From linac to wiggler

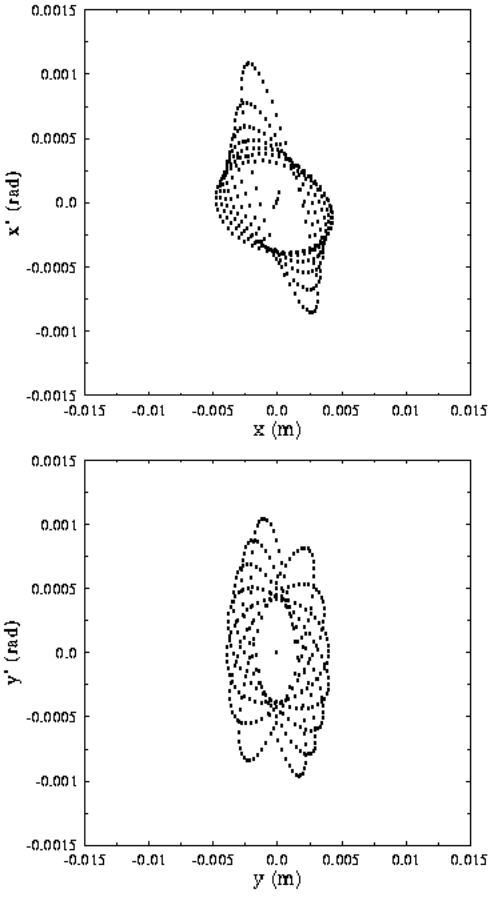

Figure 3b: From wiggler to linac

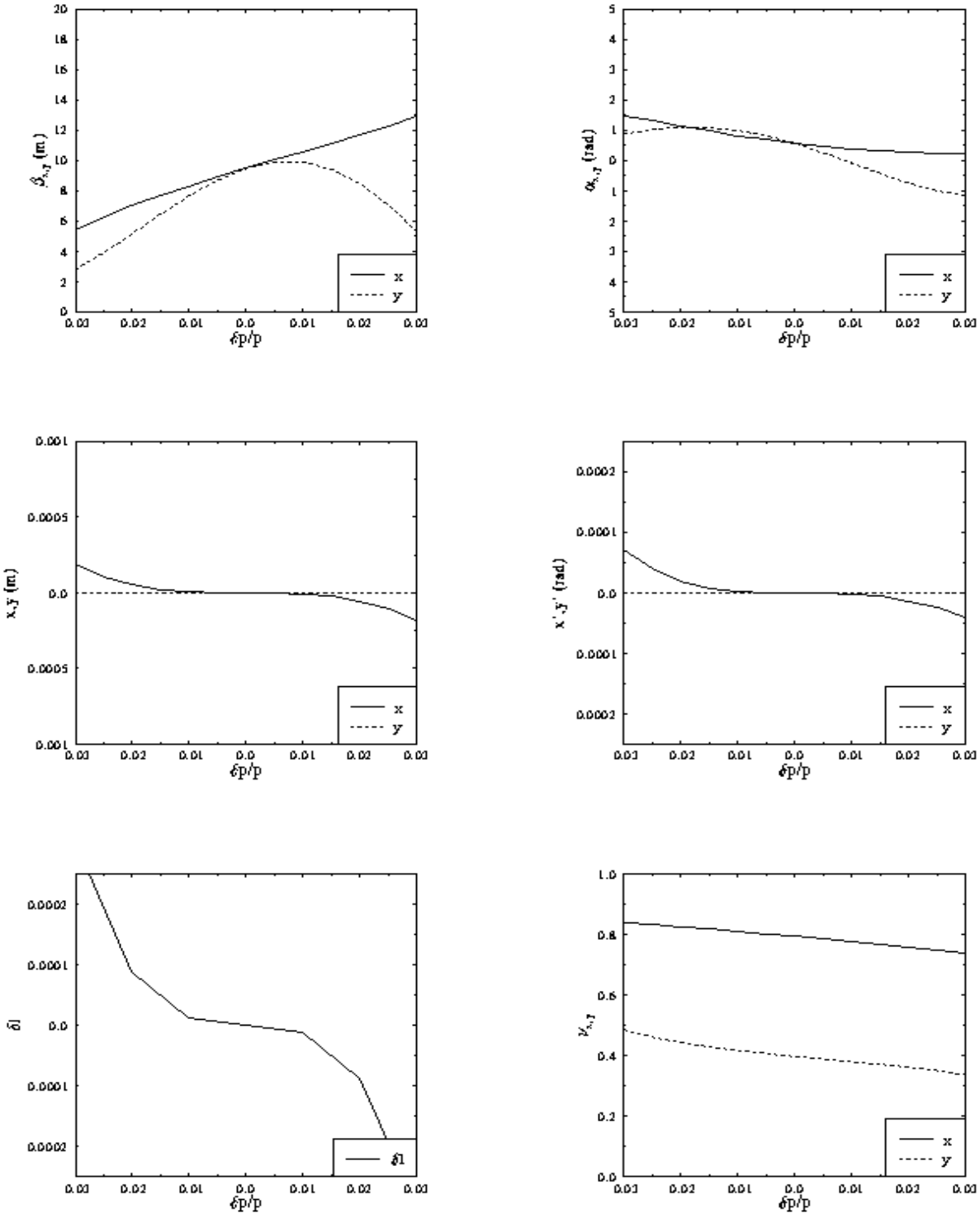

Figure 5a: Result of momentum scan using “detailed chromatic analysis” from wiggler to linac. Beam full momentum spread in this region is 5%.

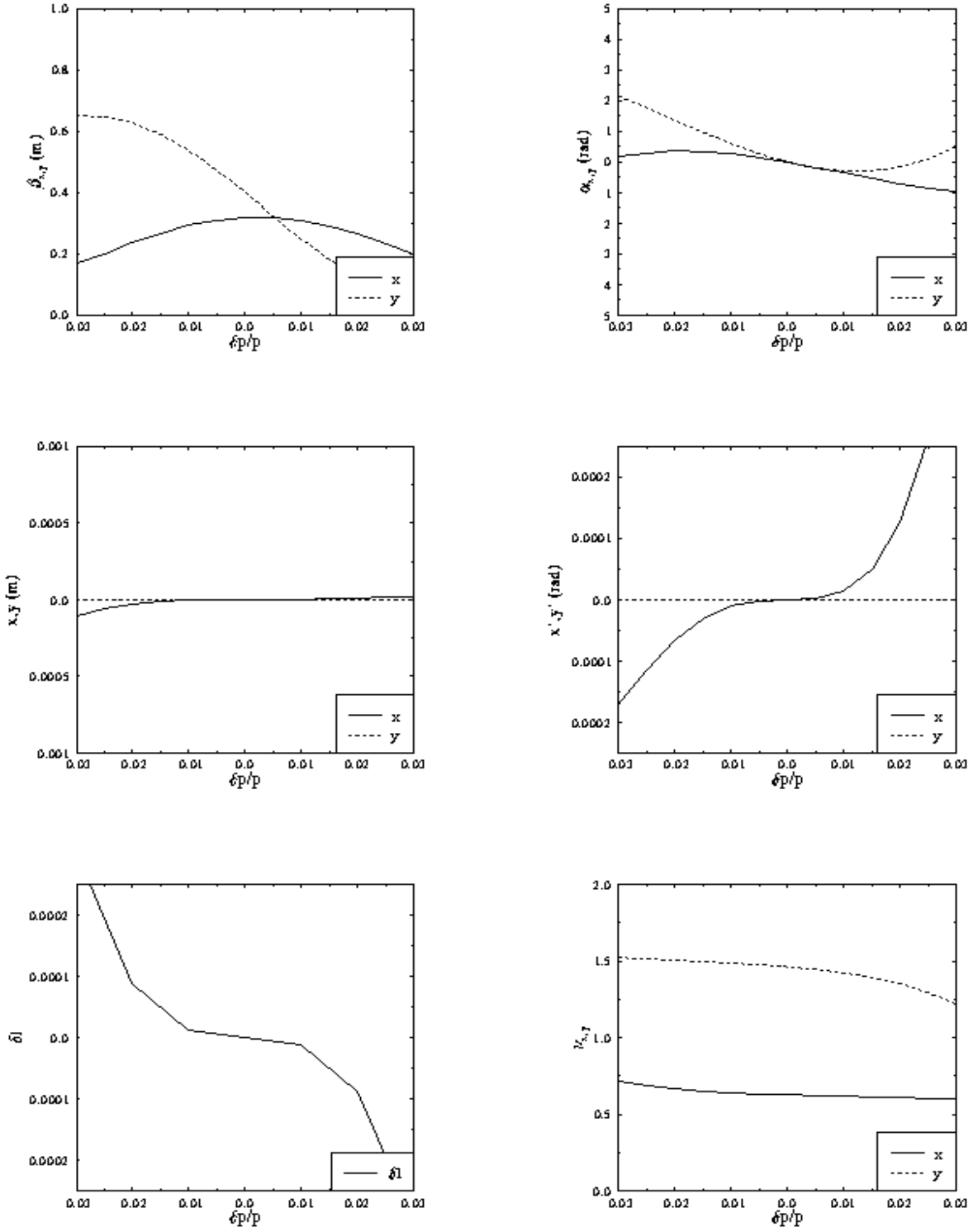

Figure 5a: Result of momentum scan using “detailed chromatic analysis” from linac to wiggler. Beam full momentum spread in this region is 2%.

Table 2: Second order transport matrix from wiggler to linac.

FIRST ORDER MATRIX

.1507330E+01	-.1674018E+01	.0000000E+00	.0000000E+00	.0000000E+00	.5634382E-15
.4612711E+00	.1511439E+00	.0000000E+00	.0000000E+00	.0000000E+00	.3747003E-15
.0000000E+00	.0000000E+00	-.3883739E+01	.1175862E+01	.0000000E+00	-.1026372E-17
.0000000E+00	.0000000E+00	-.7694373E-01	-.2341879E+00	.0000000E+00	-.2033425E-19
.1387779E-16	-.2498002E-15	.0000000E+00	-.1734723E-17	.1000000E+01	-.3095397E-15
.0000000E+00	.0000000E+00	.0000000E+00	.0000000E+00	.0000000E+00	.1000000E+01

SECOND ORDER TERMS

-.4051712E+00	.1871221E+00	.4842553E-16	.2915234E-02	.0000000E+00	-.4393956E+02
	.1707197E+02	.1272639E-16	-.8265586E-03	.0000000E+00	-.1474689E+02
		-.7774857E+02	.8035521E+02	.0000000E+00	-.4109389E-16
			-.1914281E+02	.0000000E+00	.2123582E-16
				.0000000E+00	.0000000E+00
					.2039688E-14
-.1202303E+00	.4055699E+00	-.9113753E-17	-.4471325E-03	.0000000E+00	.5472178E+01
	.4989748E+01	-.3760095E-17	-.4868183E-04	.0000000E+00	-.6184205E+01
		-.9707204E+00	.8238057E+01	.0000000E+00	-.5130729E-18
			-.3904987E+01	.0000000E+00	.2177107E-17
				.0000000E+00	.0000000E+00
					-.3094747E-14
-.3920031E-02	.1195757E-02	-.1482740E+02	-.6115896E+01	.0000000E+00	-.3918501E-17
	.4008477E-03	-.6927091E+02	.4275296E+02	.0000000E+00	-.1830652E-16
		.1366119E-16	.1817671E-16	.0000000E+00	.8023260E+01
			.1095688E-16	.0000000E+00	.2510074E+02
				.0000000E+00	.0000000E+00
					.2067707E-17
-.7766274E-04	.2369005E-04	-.1800863E+02	.6225311E+01	.0000000E+00	-.4759217E-17
	.7941501E-05	-.8260705E+01	.7525077E+01	.0000000E+00	-.2183092E-17
		.2706523E-18	-.1451304E-17	.0000000E+00	-.2909703E+02
			-.6256452E-20	.0000000E+00	.8823066E+01
				.0000000E+00	.0000000E+00
					-.7690639E-17
.1460586E+02	-.3291504E+01	-.1001484E-31	-.4336809E-18	.0000000E+00	-.2638802E-13
	.6164178E+01	.4237046E-32	.1761829E-18	.0000000E+00	.5844500E-14
		.5696071E+02	-.3242561E+02	.0000000E+00	.3009744E-16
			.7988813E+01	.0000000E+00	-.9030042E-17
				.0000000E+00	.0000000E+00
					.2702374E-15

High-Order Optics Design; Aberration Analysis. We have explored the nonlinear behavior of the machine using the DIMAD “detailed chromatic analysis”, “line geometric aberrations” and “tracking” operations. These studies indicate that the baseline design meets all requirements stated above.

Figure 5 presents the results of momentum scans of transport system behavior from linac to wiggler and from wiggler to linac. The first series, from linac to wiggler, demonstrates the beam remains well matched to the wiggler over the full 2% incoming momentum spread. The second series, from wiggler to linac, shows that the full 5% momentum spread of the beam remains well confined during transport from wiggler to linac.

Second order transport matrices from linac to wiggler and from wiggler back to the linac for sextupole-corrected transport are given in Tables 1 and 2. In both cases, first and second order matrix elements remain small, indicating good control over chromatic and geometric aberrations. The matrix in Table 2 is for a “nominal” isochronous and achromatic transport from wiggler back to the reinjection point.

Table 1: Second order transport matrix from linac to wiggler

FIRST ORDER MATRIX

-.5566979E-01	-.1233553E+01	-.1182020E-16	-.1926064E-16	.0000000E+00	-.3666339E-17
.6370685E+00	-.3846656E+01	-.5042062E-16	-.8499515E-16	.0000000E+00	.5704876E-15
.8757855E-17	.1491038E-16	-.2275149E+00	.4730153E+00	.0000000E+00	.2642743E-18
-.5154187E-16	-.8392264E-16	.1586415E+00	-.4725141E+01	.0000000E+00	.0000000E+00
-.2775558E-15	.2407412E-34	-.4336809E-18	-.8673617E-18	.1000000E+01	-.1194550E-14
.0000000E+00	.0000000E+00	.0000000E+00	.0000000E+00	.0000000E+00	.1000000E+01

SECOND ORDER TERMS

-.1070388E+01	-.7567863E+01	.2358143E-04	-.7023735E-03	.0000000E+00	-.1424397E+01
	-.1270906E+02	-.6571638E-04	.1957364E-02	.0000000E+00	.6703343E+01
		-.1918639E-01	.8916434E+01	.0000000E+00	.1161118E-15
			.2552017E+02	.0000000E+00	.1951513E-15
				.0000000E+00	.0000000E+00
					-.1612235E-14
-.6264453E+01	-.4309319E+02	.1328872E-04	-.3958049E-03	.0000000E+00	-.7592218E+01
	-.7053804E+02	-.5829280E-03	.1736252E-01	.0000000E+00	-.1465198E+03
		.4576592E+01	.5653940E+02	.0000000E+00	-.1289678E-14
			.1111660E+03	.0000000E+00	-.2090856E-14
				.0000000E+00	.0000000E+00
					.7561628E-15
.4968046E-04	-.4684607E-03	-.2237946E+01	-.1438965E+02	.0000000E+00	.2050101E-15
	-.1469615E-02	-.1347507E+02	-.3449520E+02	.0000000E+00	.3198517E-15
		-.1035091E-15	-.2857584E-15	.0000000E+00	.3106972E+01
			-.2138589E-15	.0000000E+00	.2659043E+02
				.0000000E+00	.0000000E+00
					.1355253E-19
.4462576E-15	.1540434E-14	.3692686E+01	.4883510E+02	.0000000E+00	.5647265E-15
	.9853229E-15	.5967190E+02	.1798486E+03	.0000000E+00	.1025884E-14
		.5548676E-15	.1965442E-14	.0000000E+00	-.3437466E+02
			.1471046E-14	.0000000E+00	-.1160139E+02
				.0000000E+00	.0000000E+00
					.0000000E+00
.6473150E+00	.3100379E+01	-.1042323E-15	.1471933E-14	.0000000E+00	-.2484464E-14
	.1056352E+03	.1861061E-14	.6221493E-14	.0000000E+00	-.2838332E-13
		.3645879E+01	-.1503818E+01	.0000000E+00	.7003523E-16
			.5896042E+02	.0000000E+00	.3778445E-16
				.0000000E+00	.0000000E+00
					-.1941769E-14

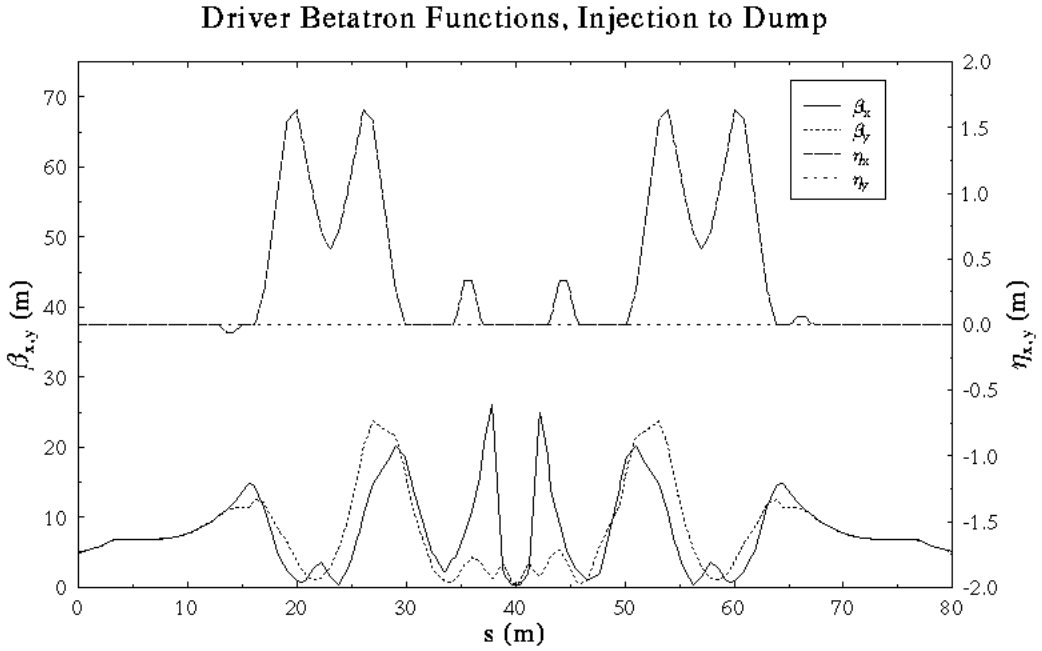

Figure 3: Beam envelope functions and dispersions from injection to extraction point. Injected beam has $\beta_x = \beta_y = 5$ m; $\alpha_x = \alpha_y = 0$ as detailed above.

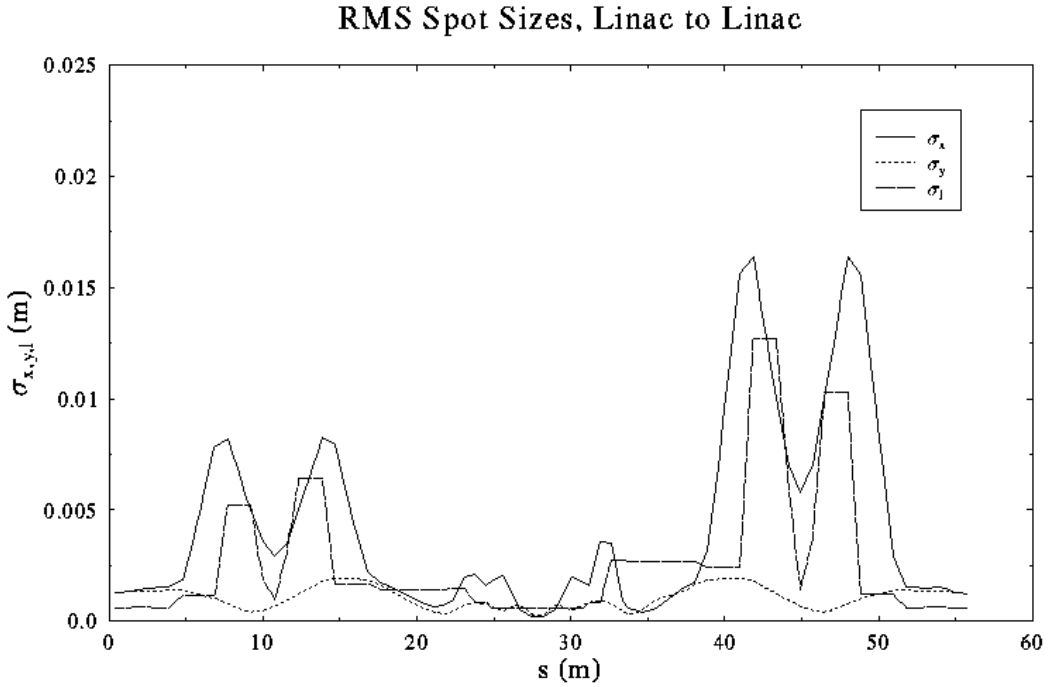

Figure 4: RMS beam spot sizes, linac to linac, for 0.16 mm-mrad rms geometric emittance throughout, 0.5% rms momentum spread from linac to wiggler and 1% rms momentum spread from wiggler to linac.

Figure 2: Schematic layout and footprint.

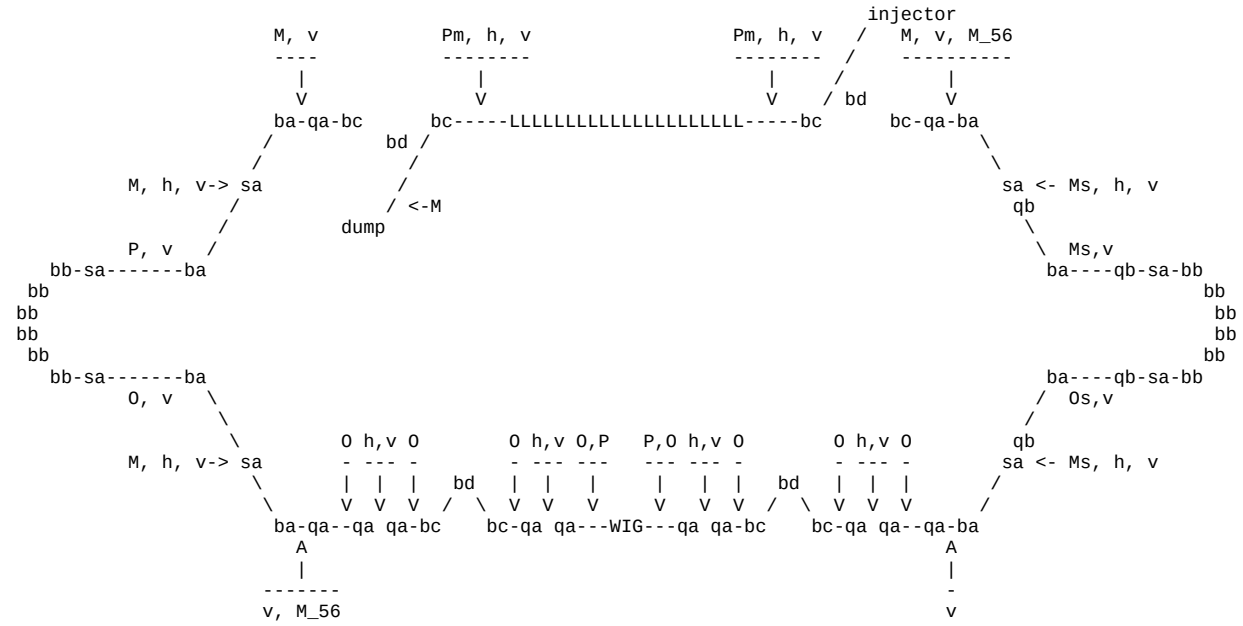

KEY:

ba	wedge bend	sa	sextupole	P	position monitor
bb	180 degree bend			Pm	multipass position monitor
bc	|| faced bend	h	horizontal corrector	M	monitor (something giving position)
bd	|| faced bend	v	vertical corrector	Ms	large aperture monitor
				M_56	M_56 monitor
qa	normal quadrupole	O	OTR monitor		
qb	trim quadrupole	Os	large aperture OTR		

Figure 2a: Detailed schematic of IR FEL baseline design.

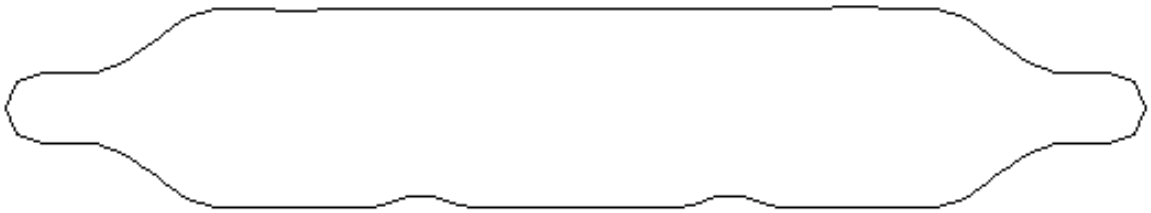

Figure 2b: Footprint of IR FEL baseline design. Cryomodule is on top leg; wiggler is centered on bottom leg.

No linac external focussing (other than the quad singlets leading and trailing the arcs) other than the quadrupole singlets leading and trailing the arcs is used in this design. Adequate beam confinement is provided by choice of injection condition, linac rf focussing, the focussing effects of the arcs proper, and the matching telescopes. The beam envelop match from the linac to the wiggler is reflectively symmetric about the wiggler center. Thus, the (β, α) value injected into the arc is mapped to $(\beta, -\alpha)$ upon reinjection into the linac, and evolves to very nearly (but not exactly) the injection point values after energy recovery [12]. Slightly different solutions (based on differing quad singlet excitations) are used in the leading and trailing telescopes so as to optimize chromatic performance.

A detailed system schematic [13] and footprint are presented in Figure 2. Typical minimum element to element distances exceed 0.5 m. The diameter (linac axis to wiggler axis distance) of the system is 5.5 m, set by varying the bend radii of the sector dipoles. As noted above, the radii of the large bends are set at 1 m for CSR control purposes. DIMAD is used to fit M_{16}, M_{26}, and M_{56} across each arc to zero by varying the bend angles (and pole face rotations - to retain the double focussing character) and separations of the small dipoles. As noted above, the M_{56} and path length of the return arc can be varied while maintaining achromaticity by appropriately imposed trim quad settings. This feature could be added to the “in” arc as an upgrade, if desired, but is not considered a feature of the baseline design.

System Performance

To date, the system performance meets the known requirements as detailed above.

Low-Order Optics Design. Beam envelope functions and dispersions propagated from the injection point (with the injection condition detailed in the requirements) through the system are presented in Figure 3. They satisfy the peak value requirement and suggest that error sensitivities, aberrations, and loss rates should be well controlled. We note that the accelerated and energy recovered solutions are, through the recirculation, slightly asymmetric. In this case, the solutions for transport to and from the wiggler are based on differing quad singlet excitations so as to optimize chromatic performance. The transport through the linac is nearly reflectively symmetric, as discussed above [14].

Figure 4 displays the rms beam spot sizes from linac end to linac start for nominal normalized emittances of 13 mm-mrad (0.16 mm-mrad geometric emittances at 40 MeV), an rms bunch length of 0.6 mm, an 0.5% rms momentum spread up to the wiggler, and an rms momentum spread of 1% downstream of the wiggler. A full six-sigma beam will, on the basis of this graph, be well contained (*i.e.*, will propagate with a full 1 cm beam stay clear in all transverse directions) in a 5 cm diameter pipe through the straight portion of the machine; larger pipe is required for the arcs (particularly the return arc) where a rectangular beam pipe of ~15 cm horizontal and 5 cm vertical acceptance is needed.

MeV beams by 5^o at a 4 m bend radius). This choice reduces the impact of the vertical focussing introduced by the rectangular dipoles that form the chicanes.

The Bates-like arcs are simple beam lines known [10] to provide large acceptance. They are half-chicanes generated by pairs of double-focussing sector dipoles (edge angles = 1/4 total bend angle), separated by a single 180^o main dipole of 1 m bend radius. The use of double-focussing dipoles provides minimization of matrix elements/beam envelope functions while providing focussing for the horizontal dispersion management necessary for achromaticity and isochronicity. Quadrupole singlets are placed upstream and downstream of the arc to provide additional degrees of freedom in beam envelope control through the arc and to/from the matching telescopes. The quad singlets are set so as to minimize chromatic variation of the beam phase space at the wiggler and at the reinjection point; they can, in principle, also be used to provide phase advance control so as to modify beam breakup thresholds, should this prove necessary.

The beam envelopes and matrix elements resulting from use of this design are modest in magnitude, thereby reducing beam size, error sensitivity, and coupling to aberrations. Four sextupoles in two families are provided for aberration control. The required momentum aperture and dispersive orbit control has been achieved with good overall chromatic and geometric aberration sensitivity by simply using these sextupoles to correct T_{166}, T_{266}, and T_{566}.

The return (energy recovery) arc has an additional four trim quadrupoles (shown in Figure 1) that can be used to vary M_{56} and/or correct dispersion errors. Use of these trims while moving the return 180^o dipole absolute longitudinal position ± 5 cm allows variation of the path length by a full rf wavelength with little impact on the energy recovered beam properties over a momentum compaction range of ± 0.25 m.

The four-quad telescopes leading and trailing the wiggler provide betatron matching over a broad range of initial conditions. In this matching, the wiggler is assumed to bend vertically and focus in the nonbending (horizontal) plane only. A pair of horizontal chicanes, moving the electron beam around optical cavity elements, are embedded in the centers of the telescopes, and contribute to the vertical focussing.

We note that this design differs from earlier efforts [11] in that no phase advance control (other than that implicitly provided by the quad singlets upstream and downstream of each arc) is provided to modify beam breakup thresholds. This reduces parts count and operational complexity, and has the added positive feature of reducing betatron mismatch and chromatic aberration levels driven by forcing the phase advance to particular values. The overall phase advance from injection point to extraction point with this simplified design falls near 4 wavelengths horizontally and 3 1/2 wavelengths vertically.

matching to wiggler periodic focussing in non-bend plane;
matching to upright phase ellipse with $\beta = 0.4$ m at center of wiggler in the bending plane.

- Achromatic transport from wiggler to linac for energy recovery, with variable momentum compaction ($|M_{56}| \leq 0.25$ m).
- Minimal parts count, maximal operational simplicity.
- Large acceptance:

  $\varepsilon_{rms} \sim 0.16$ mm-mrad geometric emittance at 40 MeV

  $\delta p/p \sim \pm 1\%$ from linac to wiggler

  $\delta p/p \sim \pm 2.5\%$ from wiggler to linac

  Here, "acceptance" refers to that region of phase space over which beam properties are "good" at the wiggler (*e.g.*, spot size variations of order 10% or less) and over which we achieve good beam *confinement* at the linac (*e.g.*, propagated phase space is well defined and regular with spot size variations of order 100% or less).

- Good beam envelope control ($\beta^{maximum} < 50$ m), which
  reduces beam size,
  reduces error sensitivity,
  reduces coupling to aberrations, and
  reduces beam loss.

Design Solution. The chosen solution is similar to an earlier design [9] and comprises a 10 MeV injector, a single cryomodule supplying 30 MeV acceleration, a Bates-like 180^o achromatic/isochronous arc bending to a four-quad telescope that matches to a wiggler. The energy-recovery transport comprises a second four-quad telescope matching wiggler to cryomodule through a second Bates-clone arc, which in this application is modified (through the introduction of trim quadrupoles) to provide variable momentum compaction with $|M_{56}| \leq 0.25$ m. The system configuration is shown in Figure 1.

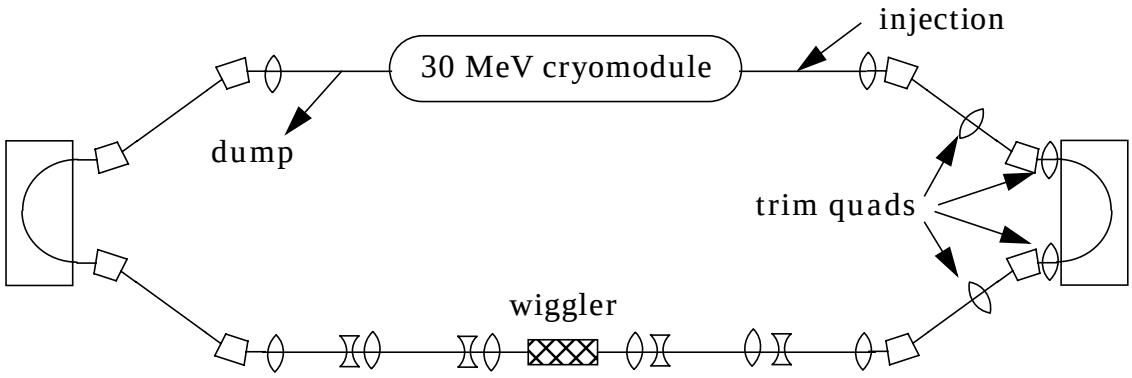

Figure 1: Conceptual design of IR FEL driver

The single 30 MeV cryomodule is preceded and followed by 2 m utility drift spaces and injection/extraction chicanes. The outboard dipoles in the chicanes bend the 10 MeV injected/extracted beams by 20^o at a 1 m bend radius (thereby bending the 40

the RF focussing present in CEBAF cavities at these low energies; details of the beam properties are given in the accompanying discussion of system performance.

This injection condition has been determined by Liu to be achievable and to provide adequate beam properties though the acceleration process, even in the presence of space charge [6].

2. Choice of Arc Design. The arc from cryomodule to wiggler must provide very good beam properties over a large momentum and geometric acceptance; the arc from wiggler to cryomodule need only provide adequate beam confinement, but must do so over the same large geometric acceptance and an extremely large momentum range. Use of similar arc configurations for both ends of the recirculator is therefore a reasonable design starting point.

Three arc configurations have been considered. The first design was an achromatic, isochronous, three-dipole "W" configuration. This was rejected almost immediately because of mechanical congestion, poor chromatic properties, and operational inflexibility (it was, for example, difficult to change overall path length and momentum compaction). The second configuration was the traditional achromatic Steffan system with variable momentum compaction. This was rejected because of poor chromatic behavior and operational inflexibility (it was difficult to change overall path length and complex to set the sextupoles for proper chromatic correction). The selected choice was a modification of the Bates recirculator arc [7].

We note that the constraints are, in this case, somewhat different than those imposed at MIT. As here, large momentum acceptance was required at Bates, but it was needed over the complete recirculation. Thus, the MIT system is symmetric about the backleg center; this allows passive suppression of some chromatic aberrations [8] that will, in the IR FEL driver, not be eliminated because of the symmetry violations imposed by the lasing process. This loss of symmetry requires additional caution to insure proper chromatic behavior is achieved for the energy recovered beam. We note that if the CSR-driven option discussed above is pursued, the symmetry in question can be recovered, providing some assistance in aberration management during the energy recovery process.

3. Matching Telescope Issues. Once the arc configuration is fixed, the performance of the matching telescopes can be readily determined. This is discussed in the following design description.

Details

Design Requirements. The transport system-specific design requirements are summarized as follows:

- Acceleration from 10 MeV to 40 MeV; transport to FEL at 40 MeV, transport back to the cryomodule at 40 MeV and energy recovery to 10 MeV
- Achromatic isochronous transport to the wiggler.
- Betatron matching into the wiggler (here assumed to focus in the nonbending plane only):

- the beam path should be such that there is space for optical cavity components at ±4 m from the wiggler center. Transverse clearances of ~20 cm (8 inches) from optical cavity axis to magnetic component are deemed adequate [5]
- space should be allocated at the design stage for diagnostic and correction system components

BBU Management. The design should provide beam breakup thresholds adequate for FEL operation at the 1 kW level. A capacity for operational modification of beam breakup thresholds by adjusting pass-to-pass transfer matrices is desirable but should not introduce undue operational complexity or additional cost.

System Design

Two basic concepts are available for the driver layout. The first has the FEL in the backleg with an arc transporting high quality beam from the linac to the wiggler with a second returning spent beam for energy recovery. The second concept has the FEL downstream of the linac, with use of the full recirculation only for energy recovery transport of the spent beam. The latter option avoids the issue of CSR driven emittance dilution, as the beam is not significantly bent before the wiggler. The former has, however, been selected for the baseline design for three reasons. First, CSR has not been confirmed to be an issue. Second, the CSR driven design has a larger footprint and is more complex operationally. Third, the CSR driven design is more costly. We therefore have generated a baseline design that is intended to be readily upgradeable to a CSR driven option at only modest cost, but which is operationally simpler and less costly than the CSR driven design.

Design Overview

Given the choice of a backleg FEL, the phase space management requirements detailed above suggest a simple driver concept comprising a cryomodule with no external focussing, an isochronous, achromatic transport arc bending to a backleg, and an achromatic return arc of variable momentum compaction bending back to the cyromodule for energy recovery. The backleg would consist of a matching telescope upstream of the wiggler, the wiggler/optical cavity assembly, and a matching telescope downstream of the wiggler.

This concept is viable provided that 1) an appropriate combination of rf focussing and injection condition can be achieved for transport through the module without external focussing, 2) arc designs can be developed that meet the required chromatic behavior without matching from or to the cryomodule, and 3) the dynamic range, acceptance, and chromatic behavior of the matching telescopes are adequate to meet the phase space management requirements. Each of these issues has been examined and (at least preliminary) solutions have been obtained.

1. Use of RF Focussing. It has been determined that injection of an upright phase ellipses ($\alpha = 0$) with beam envelope function of 5 m in both transverse planes provides good beam properties through a single cryomodule during acceleration from 10 MeV to 40 MeV. Good beam confinement without external focussing is provided by

across the 2% full momentum spread of the beam
3. geometric aberration degradation of the beam spot size will remain at or below ~10% over the full 2% momentum spread of the beam.

Energy Recovery. To minimize rf power costs and radiation from the electron beam following the FEL, the system must support energy recovery of the "spent" electron beam from 40 MeV to 10 MeV; this is to be done with sufficiently low beam loss to allow safe machine operation. (See below for further comments in this regard.) This requirement implies the transport from wiggler to cryomodule for energy recovery will provide good beam confinement:

- the system will support betatron matching from wiggler to cryomodule,
- the system will provide the same emittance acceptance as the cryomodule to wiggler transport, and
- the system will provide beam containment for $\pm 2.5\ \%$ momentum offsets to accommodate the 5% relative momentum spread of the spent electron beam. This implies:
  1. the energy recovery transport will be dispersion suppressed, and
  2. the energy recovery transport will provide variable momentum compaction for beam energy compression during energy recovery. Estimates based on an analytic model [3] indicate that M_{56} values in the range of a ± 0.25 m range will provide adequate compression.

Low Beam Loss Rates. The system must support FEL operation and energy recovery at beam loss rates allowing safe and stable operation. This implies, for the emittances and momentum spreads discussed above and mechanically reasonable components (maximum apertures not exceeding ~10 to 20 cm; see discussion below)

- the peak beam envelope functions in the system will not exceed ~50 m, and
- the peak dispersions will not exceed ~2 m.

CSR Management. Coherent synchrotron radiation (CSR) has of late become an issue of concern in the generation of low emittance, low energy, high brightness electron beams [4]. To provide some control of this effect, all bend radii will be at or in excess of 1 m. Beyond this, the design should admit modifications that would allow FEL placement before any bending for energy recovery, so as to avoid the CSR issue altogether.

Mechanical Rationality. The system should be mechanically simple and, if possible, use magnetic components in, or similar to those in, the present CEBAF inventory. Element lengths, strengths, and apertures should be on scales reasonable for a low energy machine (*e.g.*, lengths of a few to several tens of centimeters, apertures of a few to a few tens of centimeters, pole tip fields from a few tens to a few hundreds of gauss). Additionally, the system should support the following features, intended to make the system mechanically simple, easily maintained, and operationally robust:

- adequate space should be provided between magnets for mechanical and electrical connections, vacuum components, alignment fixtures, *etc.* The minimum longitudinal spacing between active field regions should typically exceed ~0.3 m.

A Baseline Design for an IR FEL Driver Accelerator

D. Douglas

Abstract

A baseline design for the beam transport system of an IR FEL driver accelerator is defined.

Requirements

Beam transport system requirements for the IR FEL driver accelerator are dictated by the following three global requirements:

- beam property requirements demanded for IR FEL operation as communicated to me by Benson and Neil [1],
- accelerator operational demands, including operational simplicity, reliability, and
- accelerator cost considerations.

The demands of FEL operation specify the beam energy and define the beam phase space properties at the wiggler. The latter two requirements drive a demand for an accelerator based on a single high gradient CEBAF cryomodule with recirculation for energy recovery, minimal parts count, and highly integrated functionality in the magnetic lattice. Design specific implications of these choices are as follows.

Energy. The beam energy will range from 10 MeV at injection to 40 MeV at the wiggler, with energy recovery to 10 MeV.

Phase Space At Wiggler. The transverse phase space at the wiggler will be defined by the needs for FEL operation with extraction of up to 1 kW of light. This implies the system should accommodate the following beam properties and manipulations:

- a 13 mm-mrad rms normalized emittance in both planes
- incoming rms momentum spread of 0.5% and full momentum spread of 2%
- betatron matching to the wiggler (here assumed to be a 40 period 5.9 kg peak field wiggler with total length of 0.72 m); beam envelope functions are to match to wiggler periodic focussing in the non-bending plane and to an upright phase ellipse at the center of the wiggler with beam envelope function value of 0.4 m in the bending plane
- transport to the wiggler is to be achromatic
- transport to the wiggler is to maintain the injected bunch length (which is adequate to allow laser operation), implying the transport should be isochronous [2].
- transport to the wiggler should not introduce optical aberrations that could degrade laser performance. Specifically:
  1. nonlinear dispersion and momentum compaction will be suppressed
  2. chromatic variation of beam spot sizes will remain at or below ~10%